be indicative of reorganization of the donor centers around copper in Cu(II)-BLM.

(vi) In aqueous phosphate buffer (pH 7), **3** is reduced at a relatively high potential (-0.27 V vs Ag/AgCl). This allows facile DTT reduction of **3** to Cu(I) species that upon oxygenation produces the $^{\bullet}OH$ radical. The $[Cu(PMA)]^{+}$-DTT-$O_2$ system induces significant amounts of double-strand breaks in plasmid DNA.

**Acknowledgment.** Financial support from the donors of the Petroleum Research Fund, administered by the American Chemical Society, at UCSC and from the NSERC of Canada at the University of Windsor is gratefully acknowledged. Part of this research was also supported by a grant from the Cancer Research Coordinating Committee of UC.

**Supplementary Material Available:** Crystal structure data for **3b** and **4** including thermal parameters for non-hydrogen atoms (Table S1), positional parameters for the hydrogen atoms (Table S2), and selected bond distances and angles associated with the perchlorate groups (Table S3) (5 pages); observed and calculated structure factors (Table S4) (11 pages). Ordering information is given on any current masthead page.

Contribution from Salutar, Inc., 428 Oakmead Parkway, Sunnyvale, California 94086, and the Department of Chemistry, University of California, Berkeley, California 94720

# Manganese(II) *N,N'*-Dipyridoxylethylenediamine-*N,N'*-diacetate 5,5'-Bis(phosphate). Synthesis and Characterization of a Paramagnetic Chelate for Magnetic Resonance Imaging Enhancement

Scott M. Rocklage,*[†] William P. Cacheris,[†] Steven C. Quay,[†] F. Ekkehardt Hahn,[‡] and Kenneth N. Raymond[‡]

*Received September 29, 1988*

The synthesis and characterization of the new ligand *N,N'*-dipyridoxylethylenediamine-*N,N'*-diacetic acid 5,5'-bis(phosphate) (DPDP, for dipyridoxal diphosphate) are described. The solution equilibrium properties of DPDP and the Mn(II), Zn(II), Cu(II), and Fe(III) complexes have been determined. log $K_{ML}$ values are 15.10, 18.95, 22.08, and 33.52 for $MnDPDP^{6-}$, $ZnDPDP^{6-}$, $CuDPDP^{6-}$, and $FeDPDP^{5-}$, respectively. Crystals of the salt $CaNa_2MnC_{22}H_{26}N_4O_{14}P_2 \cdot 21H_2O$ (**1**) are monoclinic, space group $C2/c$ (No. 15), with $a = 24.490$ (3) Å, $b = 14.440$ (2) Å, $c = 30.703$ (4) Å, $\beta = 112.747(12)°$, and $Z = 8$. The asymmetric unit contains 1 MnDPDP anion, 1 calcium cation, 2 sodium cations, and 21 water molecules. The manganese(II) oxidation state was confirmed by the stoichiometry, by the Mn-O1, Mn-O8, Mn-N2, and Mn-N4 bond distances, and by magnetic susceptibility measurements. In vivo applications of MnDPDP for magnetic resonance imaging enhancement are discussed.

## Introduction

We recently reported the structural and thermodynamic characterization of manganese(II) *N,N'*-dipyridoxylethylenediamine-*N,N'*-diacetate, MnPLED.[1] This complex represented an example of a Mn(II) hexadentate chelate that is stable to hydrolysis at neutral pH. This was part of our research program aimed at the preparation and characterization of paramagnetic chelates containing biologically relevant organic moieties for NMR imaging contrast enhancement, in which we are now investigating the coordination chemistry of ligands derived from pyridoxal 5-phosphate (PLP), the coenzyme of vitamin $B_6$. MnPLED was found to have a thermodynamic stability constant slightly lower than that of MnEDTA (log $K$ of 12.56 vs 13.95) and to have limited aqueous solubility (<50 mM). For these reasons derivatives have been sought that would overcome these deficiencies.

Pyridoxal 5-phosphate containing enzymes participate in the deamination, decarboxylation, transamination, racemization, and transsulfurization of amino acids and in the metabolism of fats and carbohydrates.[2] A number of studies have demonstrated that nonenzymatic transamination is catalyzed by certain metal ions in ternary model systems containing an amino acid, carbonyl compound, and metal ion.[3-5] A general mechanism for PLP-catalyzed reactions proposed by Metzler et al.[6] is the formation of an intermediate Schiff base from PLP and an amino acid. Subsequent work has shown that the metal ion stabilizes the aldimine and ketamine Schiff base forms by chelation;[7-10] NMR studies of binary PLP-metal ion systems with paramagnetic shift agents have demonstrated coordination of metal ions via the phosphate moiety with limited participation by the aldehyde.[11-13]

The novel ligand described in this paper, *N,N'*-dipyridoxylethylenediamine-*N,N'*-diacetic acid 5,5'-bis(phosphate), forms stable, highly water-soluble hexadentate chelates involving the PLP hydroxy groups. Herein, we report the synthesis and characterization of this new ligand and the solution equilibrium properties with Mn(II), Cu(II), Zn(II), and Fe(III) ions.

## Experimental Section

**Synthesis of *N,N'*-Dipyridoxylethylenediimine 5,5'-Bis(phosphate).** A 12-L three-neck round-bottom flask fitted with a mechanical stirrer was charged with 530.8 g (2.0 mol) of pyridoxal 5-phosphate and 2.5 L of $CH_3OH$. The mixture was stirred while 800 mL of 5 N NaOH was added. When a homogeneous yellow solution was obtained (in ca. 15 min), 67 mL (1.0 mol) of 1,2-ethylenediamine was added and a bright yellow precipitate of the bis(imine) formed immediately. The yellow slurry was stirred for 1 h and subsequently used without isolation for the next step.

**Synthesis of *N,N'*-Dipyridoxylethylenediamine 5,5'-Bis(phosphate).** The bis(imine) slurry from above was diluted with 2.5 L of water and

[†] Salutar, Inc.
[‡] University of California.

(1) Rocklage, S. M.; Sheffer, S. H.; Cacheris, W. P.; Quay, S. C.; Hahn, E. F.; Raymond, K. N. Structural and Thermodynamic Characterization of Manganese(II) *N,N'*-Dipyridoxylethylenediamine-*N,N'*-diacetate. *Inorg. Chem.* **1988**, *27*, 3530-3534.
(2) Dolphin, D.; Poulson, R.; Avramovic, O. Vitamin B6 Pyridoxal Phosphate, Chemical, Biochemical, and Medical Aspects. *Coenzymes and Cofactors*; Wiley-Interscience: New York, 1986; Vol. 1, Part B.
(3) Snell, E. E.; Fasella, P. M.; Braunstein, A.; Rossi-Fanelli, A. *Chemical and Biological Aspects of Pyridoxal Catalysis*; Macmillan Co.: New York, 1963; p 1.
(4) Bruice, T. C.; Benkovic, S. J. *Bioorganic Mechanisms*; W. A. Benjamin, Inc.: Reading, MA, 1966; Vol. 2, Chapter 8.
(5) Felty, W. L.; Ekstrom, C. G.; Leussing, D. L. *J. Am. Chem. Soc.* **1970**, *92*, 3006-3011.
(6) Metzler, D. E.; Ikawa, M.; Snell, E. E. *J. Am. Chem. Soc.* **1954**, *76*, 648.
(7) Langohr, M. F.; Martell, A. E. *J. Chem. Soc., Chem. Commun.* **1977**, 343.
(8) Langohr, M. F.; Martell, A. E.; Tatsumoto, K. *Inorg. Chim. Acta* **1985**, *108*, 105.
(9) Szpoganicz, B.; Martell, A. E. *Inorg. Chem.* **1986**, *25*, 327-332.
(10) Martell, A. E.; Taylor, P. *Inorg. Chem.* **1984**, *23*, 2734-2735.
(11) Narasinga Rao, B. N.; Ramakrishnan, C.; Balaram, P. *J. Biosci.* **1979**, *1*, 35-47.
(12) Viswanathan, T. S.; Swift, T. J. *Can. J. Chem.* **1979**, *57*, 1050-1055.
(13) Viswanathan, T. S.; Swift, T. J. *Can. J. Chem.* **1980**, *58*, 1118-1124.

0020-1669/89/1328-0477$01.50/0 

500 mL of $CH_3OH$. The homogeneous solution was thoroughly sparged with nitrogen through a fritted gas-delivery tube and 21 g of 5% Pt/C added. Nitrogen was aspirated from the flask head space through a three-way valve. Hydrogen was passed through the solution via the gas-delivery tube while excess hydrogen was vented with a three-way valve into a balloon. The hydrogen was fed into the flask with vigorous stirring for 3–4 h at such a rate that excess hydrogen filled the balloon, which was slowly vented into the hood as necessary. The reaction was followed by reverse-phase HPLC (DyChrom ODS-L, 10 $\mu$, 4.6 × 250 mm; mobile phase, 0.02 M $NaH_2PO_4$, 0.2% $Et_4NOH$, $H_3PO_4$ to pH 2.7) until completion. When the reaction was complete, the flask was sparged with nitrogen to remove the unreacted hydrogen. The slurry was filtered through Celite, and the filtrate was concentrated in vacuo (60 °C) to ca. 1300 mL and used directly in the next step. Alternatively, the diamine could be isolated by acidification to pH 3 with 88% $HCO_2H$ to yield an off-white microcrystalline solid in >90% yield. $^1H$ NMR in $D_2O$/NaOD (Bruker AM250, ppm from TMS): 7.42 (s, 2 H, py *H*), 4.53 (d, 4 H, $CH_2OP$, $J_{PH}$ = 3.93 Hz), 3.94 (s, 4 H, $NCH_2$-py), 2.82 (s, 4 H, $NCH_2CH_2N$), 2.11 (s, 6 H, py-$CH_3$).

**Synthesis of *N*,*N*′-Dipyridoxylethylenediamine-*N*,*N*′-diacetic Acid 5,5′-Bis(phosphate) (DPDP).** The solution from above was placed in a 2-L three-neck round-bottom flask equipped with two addition funnels, pH electrode, thermometer, and stir bar. NaOH (200 g, 5.0 mol) and $BrCH_2CO_2H$ (280 g, 2.0 mol) were each dissolved in 450 mL of water and the resulting solutions placed in the two addition funnels. The solution of NaOH was added to the stirring diamine solution to bring the pH to ca. 11, which raised the temperature to 40 °C. The temperature was maintained at 40–45 °C, and the $BrCH_2CO_2H$ and NaOH solutions were added concurrently over the course of 3 h. The pH was maintained at 11 during the addition. The reaction was followed by HPLC (conditions as above except the buffer was run with a 0–100% $CH_3OH$ gradient over 13 min). Rohm & Haas IR-120H acid resin (2.6–3.0 kg) was added to lower the pH from 11.1 to 3.1. The resin was removed by filtration and washed with 600 mL of water. The pH of the filtrate was ca. 3.3. $HCO_2H$ (97%, 50 mL) was added, and the pH dropped to 3.0. The solution was heated to 35–40 °C, 500 mL of isopropyl alcohol was added, with a few seed crystals, and the solution was allowed to cool to room temperature overnight. The crude product was isolated by filtration, washed with 1 L of water, and dried in vacuo at 50 °C to yield 160 g of a white microcrystalline powder.

**DPDP Recrystallization.** A 160-g amount of DPDP was dissolved in $HCO_2H$ (75–80%, 200 mL) with gentle heating to 50–60 °C. The warm, slightly gray, solution was filtered through a medium frit and the filtrate diluted with cold water to a total volume of 2.2 L. The mixture was allowed to stand for 5–6 h at ambient temperature. DPDP·$2H_2O$ was isolated by filtration and washed with 300 mL of cold water. The damp solid was dissolved in $HCO_2H$ (75–80%, 175 mL) with gentle heating as described above and diluted with water to a total volume of 2 L. The product was allowed to crystallize for 5–6 h at ambient temperature, collected by filtration, washed with 250 mL of water, and dried in vacuo at 60 °C to yield 130 g of DPDP·$2H_2O$ (20% overall yield based upon pyridoxal 5-phosphate). Analysis by HPLC demonstrated that the material was 98–99% pure. $^1H$ NMR in $D_2O$/NaOD (at pD = 6.34, Bruker AM250, ppm from TMS): 7.53 (s, 2 H, py *H*), 4.51 (d, 4 H, $CH_2OP$, $J_{PH}$ = 5.85 Hz), 3.90 (s, 4 H, $NCH_2$-py), 3.21 (s, 4 H, $CH_2COOH$), 2.76 (s, 4 H, $NCH_2CH_2N$), 2.06 (s, 6 H, py-$CH_3$). TGA (50–160 °C, 10°/min, $N_2$): calcd for dihydrate, 5.34%; found, 5.50% (average of three runs). Anal. Calcd (found) for $C_{22}H_{32}N_4O_{14}P_2$·$2H_2O$: C, 39.18 (39.25); H, 5.38 (5.26); N, 8.31 (8.18).

**Synthesis of Manganese(II) *N*,*N*′-Dipyridoxylethylenediamine-*N*,*N*′-diacetate 5,5′-Bis(phosphate), MnDPDP. Method 1—Solution.** DPDP (6.75 g, 10.0 mmol) was dissolved in ca. 10 mL of degassed water containing NaOH (1.20 g, 30.0 mmol). $MnCl_2$·$4H_2O$ (1.98 g, 10.0 mmol) was added with stirring to the colorless DPDP solution; the pH dropped to ca. 3 as the solution turned yellow. NaOH (1.20 g, 30 mmol) in 10 mL of water was added; the pH increased to ca. 7.5. Solutions of $MnH_2DPDP^{2-}$ prepared in this manner were used for solution equilibria and magnetic studies.

**Method 2—Crystalline Solid.** The extremely high water solubility of MnDPDP made the complex difficult to crystallize from aqueous solutions. The addition of calcium salts induced crystallization, and X-ray-quality crystals were obtained. A 150-mg amount of $CaCl_2$·$2H_2O$ was added to 10 mL of the $MnH_2DPDP^{2-}$ solution, and the clear orange solution was allowed to stand at room temperature. Air-stable orange-yellow crystals, which lose waters of hydration upon standing in dry air, were isolated by filtration. Anal. Calcd (found) for $C_{22}H_{26}N_4O_{14}P_2CaNa_2Mn$·$21H_2O$: C, 23.02 (23.25); H, 5.62 (5.19); N, 4.88 (5.19); P, 5.40 (5.06); Mn, 4.78 (4.90).

**X-ray Data Collection for 1.** A suitable crystal of **1** with the dimensions 0.50 × 0.35 × 0.19 mm was mounted in a thin-walled glass capillary for data collection. The data collection details for **1** were similar to those reported for the earlier MnPLED·$4H_2O$ complex;[1] the differences in the data collection will be described here. The symmetry of the crystal lattice (monoclinic) and preliminary cell constants were obtained from a series of precession photographs. A three-dimensional search on an Enraf-Nonius CAD-4 diffractometer,[14,15] followed by a Delaunay reduction using the program TRACER,[16] gave a monoclinic *C*-centered cell. Final cell parameters were obtained from the angular settings of 24 high-angle reflections (27.2° ≤ 2$\theta$ ≤ 28.6°). All data $h,k,\pm l$ with $h + k = 2n$ were collected in the 2$\theta$ range 2° ≤ 2$\theta$ ≤ 45° by using the $\omega$-scan technique (this scan mode was selected because of the long unit cell edges). Orientation and intensity control reflections (2,−2,−20), (−5,−5,−13), and (12,−2,−18) were monitored as described earlier.[1,15] Crystal reorientation was required four times during the data collection. Azimuthal scans were recorded for five reflections at the end of the data collection. Final crystal and data collection details are summarized in Tables I and IS.[22]

**Table I.** Crystallographic Data for $CaNa_2MnDPDP$·$21H_2O$

| | |
|---|---|
| $CaNa_2MnC_{22}H_{22}N_4O_{14}P_2$·$21H_2O$ | space group $C2/c$ (No. 15) |
| mol mass 1151.74 amu | $T$ = 25 °C |
| $a$ = 24.490 (3) Å | $\lambda$(Mo K$\alpha$) = 0.71073 Å |
| $b$ = 14.440 (2) Å | $\mu$ = 5.29 cm$^{-1}$ |
| $c$ = 30.703 (4) Å | transmission coeff = 0.97–0.98 |
| $\beta$ = 112.747 (12)° | $R(F_o)$ = 4.75% |
| $V$ = 10013 (4) Å$^3$ | $R_w(F_o)$ = 7.21% |
| $Z$ = 8 | |

**Structure Solution and Refinement for 1.** The raw intensity data were reduced to structure factors.[15] No decay correction was applied (decay of standard reflections was −0.2% in the 112 h of X-ray exposure time). An empirical absorption correction based on five $\psi$ scans was applied (maximum and minimum correction factors 1.0 and 0.979).

The Laue symmetry and systematically absent reflections ($h0l$, $l = 2n + 1$) define the space group to be either $Cc$ (No. 9) or $C2/c$ (No. 15); the latter was confirmed by the structure analysis. Systematically absent reflections and all redundant data ($0kl$, $l < 0$) were removed from the data set, leaving 6548 unique data. The structure was solved by direct methods (MULTAN 11/82[16]), followed by difference Fourier and least-squares refinement.[17–20] A difference Fourier map calculated after all atoms in the structure model had been refined with anisotropic thermal parameters revealed the positions of all hydrogen atoms in the DPDP ligand and some of the water hydrogen atoms. Hydrogen atoms of the ligand were added at calculated positions ($d$(C–H) = 0.95 Å, $d$(N–H) = 0.87 Å[21]) with isotropic $B$'s (Å$^2$) 1.3 times larger than the $B_{eq}$ of the atom to which they are bonded. Water hydrogen atoms were added at the positions obtained from the difference Fourier map with an isotropic $B$ value of 4.0 Å$^2$. No hydrogen parameters were refined.

Hydrogen atoms for the water molecules O30–O36 could not be identified. Some oxygen atoms of the water molecules (O32–O36) showed rather larger thermal parameters; these were atoms that did not coordinate to any cation. Refinement with partial site occupancies was unsuccessful, presumably due to the large thermal motion of these atoms. A test for secondary extinction was negative. Nine strong reflections, presumably suffering from peak overlap, were not included in the least-squares procedure.

The quantity minimized by the least-squares program was $\sum w(|F_o| - |F_c|)^2$, where $w$ is the weight of a given observation.[17] Atomic scattering factors for the neutral atoms were used,[18] and all non-hydrogen scattering factors were corrected for both the real and imaginary components of anomalous dispersion.[19] The final residuals for 605 variables refined against 5488 data with $F_o^2 \geq 3\sigma(F_o^2)$ were $R$ = 4.75%, $R_w$ = 7.21%, and GOF = 3.60. The $R$ value for all 6548 unique data is 6.83%. Inspection of the residuals ordered in ranges of (sin $\theta$)/$\lambda$, $|F_o|$, and parity and value

(14) *CAD-4 Operation Manual*; Enraf Nonius: Delft, The Netherlands, Nov 1977 (updated Jan 1985).
(15) For experimental details of data collection and processing, see: Eigenbrot, C. W.; Raymond, K. N. *Inorg. Chem.* **1982**, *21*, 2653.
(16) *Structure Determination Package User's Guide*; B. A. Frenz and Associates: College Station, TX 77840, 1982.
(17) $R = \sum||F_o| - |F_c||/\sum|F_o|$, $R_w = [\sum w(|F_o| - |F_c|)^2/\sum wF_o^2]^{1/2}$, and GOF = $[\sum w(|F_o| - |F_c|)^2/(n_o - n_v)]^{1/2}$, where $n_o$ is the number of observations, $n_v$ is the number of variables, and the weights $w$ are given by $w = 4F_o^2/\sigma(F_o^2)$.
(18) Cromer, D. T.; Waber, J. T. *International Tables for X-ray Crystallography*; Kynoch Press: Birmingham, England, 1974; Vol. IV, Table 2.2B.
(19) Cromer, D. T. Reference 18, Table 2.3.1.
(20) Johnson, C. K. Report ORNL-3794; Oak Ridge National Laboratory: Oak Ridge, TN, 1965.
(21) Churchill, M. R. *Inorg. Chem.* **1973**, *12*, 1213.

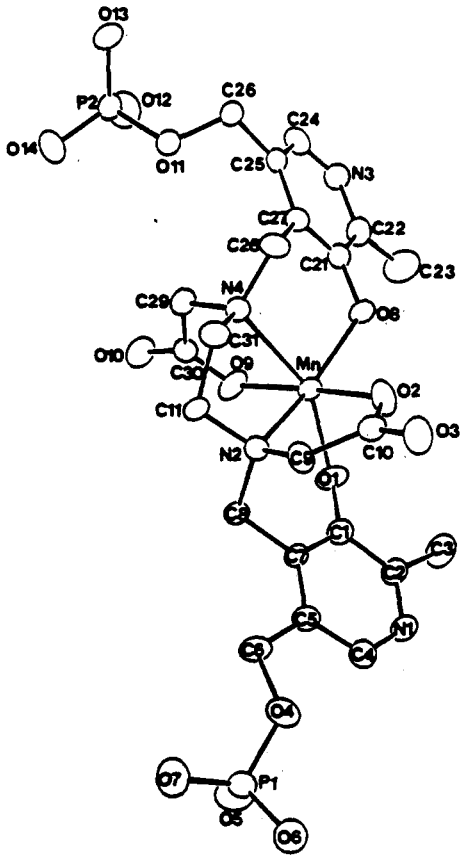


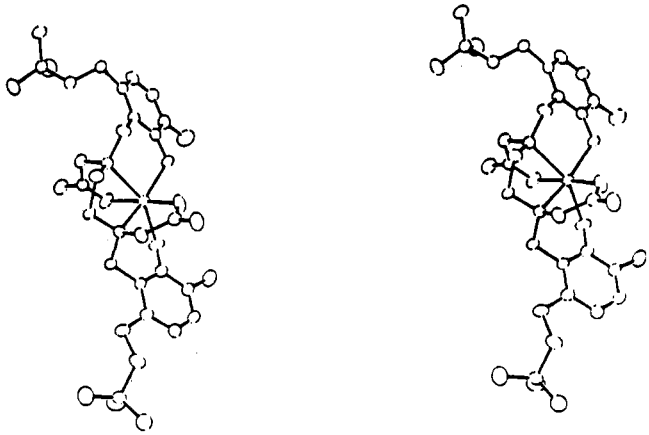

**Figure 1.** (Top) Plot of one molecule of $CaNa_2MnDPDP{\cdot}21H_2O$ (**1**) with the crystallographic numbering scheme. Water molecules and Ca, Na, and hydrogen atoms have been ommitted for clarity. The ellipsoids in this and all other plots were scaled to represent the 50% probability surface. (Bottom) Stereoview of the complex.

for the individual index showed no unusual features or trends. The largest positive peak in the final difference Fourier map had an electron density of 0.93 e/Å$^3$. The largest negative peak in this map had an intensity of 0.49 e/Å$^3$.

Final positional and thermal parameters for all atoms are listed in Tables II and IIS.[22] The atomic numbering scheme followed in these listings is identified in Figures 1–3. Tables III and IIIS[22] list intramolecular bond distances and angles. Selected parameters of intramolecular and intermolecular hydrogen bonds as well as some nonbonding Mn–O(water) distances are given in Tables IVS[22] and IV, respectively. The calculation of some least-squares-plane parameters is presented in Table VS.[22] General temperature factor expressions ($B$'s) and root-mean-square amplitudes of vibration are given in Tables VIS[22] and VIIS,[22] respectively. Values of calculated and observed structure factor amplitudes are listed in Table VIIIS.[22] Various views of the molecule, and the coordination geometry around the Ca and Na cations, are presented in Figures 1–3 (ORTEP drawings[20]).

(22) Supplementary material; see paragraph at end of paper.

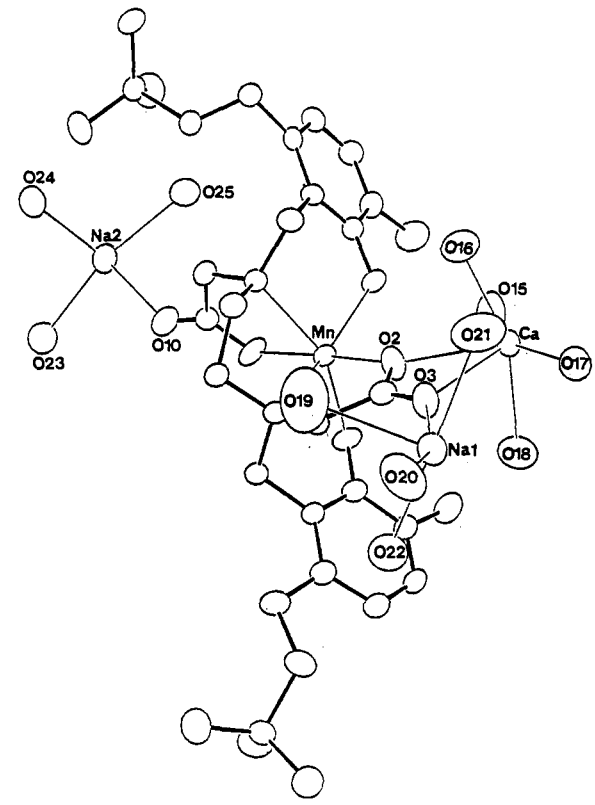


**Figure 2.** The contents of the asymmetric unit for **1** including the Na and Ca cations and all coordinating water molecules.

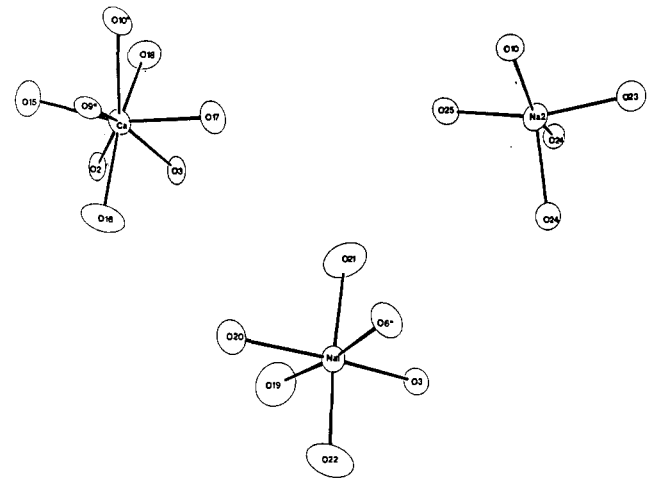

**Figure 3.** (Left) Coordination geometry of the calcium cation. (Middle) Coordination geometry of the Na1 cation. (Right) Coordination geometry of the Na2 cation. Key: (*) $^1/_2 - x, ^1/_2 + y, ^1/_2 - z$; (′) $-x, -y, -z$; (″) $^1/_2 - x, ^1/_2 - y, 1 - z$.

**Potentiometric Measurements.** The potentiometric data were measured with an automatic titrator system that has been described in detail previously.[1] The pH electrode was calibrated by several pH buffer solutions in the pH range 2–12. Values of 0.78 for hydrogen ion activity coefficient and 13.77 for $pK_w$ were obtained by monitoring the pH of several standard HCl and NaOH solutions at an ionic strength of 0.10 M (NaCl).

All titrations were carried out at an ionic strength of 0.10 M (NaCl). Sample solutions in the concentration range (3–5) $\times 10^{-3}$ M for metal ion and ligand were prepared by adding solid ligand (>99.5% pure by titration), standardized metal chloride stock solution, and NaCl to a volumetric flask and diluting to volume. An aliquot of the sample solution was then placed in the titration vessel, and the pH was adjusted by addition of a known volume of standard base. The titrations were then performed at 25.0 °C (±0.1 °C) under a nitrogen atmosphere with 0.1000 M HCl as the titrant to minimize ionic strength change during the course of the titration. Each titration was controlled by a BASIC

**Table II.** Positional Parameters and Isotropic Equivalent Thermal Parameters for $CaNa_2MnDPDP{\cdot}21H_2O$[a]

| atom | x | y | z | B, Å² |
|---|---|---|---|---|
| Mn | 0.20213 (2) | 0.23352 (4) | 0.24356 (2) | 1.86 (1) |
| Ca | 0.28677 (4) | 0.47711 (6) | 0.32896 (3) | 2.49 (2) |
| P1 | 0.20259 (4) | −0.03576 (8) | 0.48611 (3) | 2.13 (2) |
| P2 | −0.02953 (4) | 0.30324 (8) | 0.01489 (4) | 2.16 (2) |
| Na1 | 0.17476 (7) | 0.4464 (1) | 0.41609 (5) | 2.63 (4) |
| Na2 | 0.05393 (7) | 0.0129 (1) | 0.05605 (6) | 3.20 (4) |
| O1 | 0.2668 (1) | 0.1448 (2) | 0.28896 (9) | 2.64 (6) |
| O2 | 0.2210 (1) | 0.3425 (2) | 0.29553 (9) | 2.88 (6) |
| O3 | 0.2083 (1) | 0.4053 (2) | 0.35603 (9) | 2.99 (7) |
| O4 | 0.2095 (1) | 0.0560 (2) | 0.4591 (1) | 3.34 (7) |
| O5 | 0.2346 (1) | −0.1130 (2) | 0.47311 (9) | 3.15 (7) |
| O6 | 0.2308 (1) | −0.0045 (2) | 0.53637 (9) | 3.67 (7) |
| O7 | 0.1378 (1) | −0.0573 (2) | 0.4706 (1) | 3.34 (7) |
| O8 | 0.2314 (1) | 0.3237 (2) | 0.20418 (9) | 2.61 (6) |
| O9 | 0.1751 (1) | 0.1200 (2) | 0.19396 (9) | 2.71 (7) |
| O10 | 0.1061 (1) | 0.0474 (2) | 0.1360 (1) | 3.17 (7) |
| O11 | 0.0139 (1) | 0.3411 (2) | 0.06588 (9) | 2.61 (6) |
| O12 | 0.0089 (1) | 0.2642 (2) | −0.0090 (1) | 3.58 (7) |
| O13 | −0.0655 (1) | 0.3853 (2) | −0.01119 (9) | 2.85 (7) |
| O14 | −0.0656 (1) | 0.2305 (2) | 0.0270 (1) | 3.27 (7) |
| O15 | 0.3217 (1) | 0.4140 (3) | 0.2728 (1) | 5.45 (9) |
| O16 | 0.2002 (2) | 0.5490 (3) | 0.2723 (1) | 6.2 (1) |
| O17 | 0.2873 (1) | 0.5797 (2) | 0.39130 (9) | 3.55 (7) |
| O18 | 0.3429 (1) | 0.3680 (3) | 0.3867 (1) | 4.83 (9) |
| O19 | 0.0626 (2) | 0.4017 (4) | 0.3610 (2) | 8.4 (2) |
| O20 | 0.1091 (2) | 0.4818 (3) | 0.4542 (1) | 5.07 (9) |
| O21 | 0.1569 (2) | 0.5982 (3) | 0.3783 (1) | 6.6 (1) |
| O22 | 0.1960 (2) | 0.2931 (3) | 0.4466 (1) | 6.1 (1) |
| O23 | 0.0354 (1) | −0.1374 (2) | 0.0791 (1) | 3.82 (8) |
| O24 | −0.0477 (1) | 0.0471 (2) | 0.0190 (1) | 3.26 (7) |
| O25 | 0.1022 (1) | 0.1442 (2) | 0.0377 (1) | 3.46 (7) |
| O26 | 0.1767 (1) | 0.7130 (2) | 0.4568 (1) | 4.07 (9) |
| O27 | −0.1804 (2) | 0.1863 (3) | −0.0339 (1) | 5.3 (1) |
| O28 | 0.0606 (2) | 0.3418 (3) | −0.0626 (1) | 4.92 (9) |
| O29 | −0.0578 (2) | −0.1106 (3) | 0.1122 (1) | 6.6 (1) |
| O30 | −0.0691 (2) | 0.2142 (3) | 0.1140 (1) | 6.3 (1) |
| O31 | −0.0297 (3) | 0.0527 (4) | 0.1659 (2) | 9.8 (2) |
| O32[b] | 0.000 | −0.0367 (7) | 0.250 | 12.3 (3) |
| O33 | 0.0705 (3) | −0.1787 (9) | 0.2292 (2) | 18.1 (4) |
| O34 | 0.0264 (4) | 0.7109 (7) | 0.3416 (3) | 16.6 (3) |
| O35[b] | 0.000 | 0.489 (1) | 0.250 | 25.9 (9) |
| O36 | 0.4080 (4) | 0.119 (1) | 0.2219 (4) | 24.9 (5) |
| N1 | 0.3382 (1) | 0.1171 (2) | 0.4128 (1) | 2.53 (8) |
| N2 | 0.1457 (1) | 0.1973 (2) | 0.2873 (1) | 1.93 (7) |
| N3 | 0.2085 (1) | 0.3671 (3) | 0.0848 (1) | 2.61 (8) |
| N4 | 0.1063 (1) | 0.2710 (2) | 0.1902 (1) | 1.91 (7) |
| C1 | 0.2739 (2) | 0.1282 (3) | 0.3325 (1) | 2.19 (9) |
| C2 | 0.3317 (2) | 0.1319 (3) | 0.3682 (1) | 2.25 (9) |
| C3 | 0.3841 (2) | 0.1516 (4) | 0.3574 (2) | 3.5 (1) |
| C4 | 0.2937 (2) | 0.0957 (3) | 0.4266 (1) | 2.5 (1) |
| C5 | 0.2375 (2) | 0.0886 (3) | 0.3938 (1) | 2.39 (9) |
| C6 | 0.1884 (2) | 0.0594 (3) | 0.4088 (1) | 3.1 (1) |
| C7 | 0.2266 (2) | 0.1067 (3) | 0.3461 (1) | 2.07 (9) |
| C8 | 0.1648 (2) | 0.1039 (3) | 0.3082 (1) | 2.40 (9) |
| C9 | 0.1525 (2) | 0.2696 (3) | 0.3236 (1) | 2.34 (9) |
| C10 | 0.1970 (2) | 0.3446 (3) | 0.3255 (1) | 2.17 (9) |
| C11 | 0.0837 (2) | 0.1929 (3) | 0.2526 (1) | 2.41 (9) |
| C21 | 0.2037 (2) | 0.3440 (3) | 0.1595 (1) | 2.03 (9) |
| C22 | 0.2364 (2) | 0.3451 (3) | 0.1308 (1) | 2.47 (9) |
| C23 | 0.3006 (2) | 0.3250 (4) | 0.1500 (2) | 3.9 (1) |
| C24 | 0.1505 (2) | 0.3879 (3) | 0.0646 (1) | 2.59 (9) |
| C25 | 0.1170 (2) | 0.3889 (3) | 0.0914 (1) | 2.12 (9) |
| C26 | 0.0528 (2) | 0.4173 (3) | 0.0670 (1) | 2.8 (1) |
| C27 | 0.1429 (2) | 0.3658 (3) | 0.1391 (1) | 1.97 (9) |
| C28 | 0.1082 (2) | 0.3646 (3) | 0.1704 (1) | 2.23 (9) |
| C29 | 0.0841 (2) | 0.1991 (3) | 0.1534 (1) | 2.30 (9) |
| C30 | 0.1237 (2) | 0.1167 (3) | 0.1618 (1) | 2.02 (9) |
| C31 | 0.0704 (2) | 0.2759 (3) | 0.2195 (1) | 2.39 (9) |

[a] The thermal parameter given for anisotropically refined atoms is the isotropic equivalent thermal parameter defined as $(4/3)[a^2\beta(1,1) + b^2\beta(2,2) + c^2\beta(3,3) + ab(\cos\gamma)\beta(1,2) + ac(\cos\beta)\beta(1,3) + bc(\cos\alpha)\beta(2,3)$, where $a$, $b$, and $c$ are real cell parameters and $\beta(i,j)$ are anisotropic $\beta$'s. [b] The following atoms lie on special positionsd and had their positional parameters fixed accordingly: O32, O35; Wyckoff position e; site symmetry $m$; site occupancy factor 0.5.

**Table III.** Intramolecular Distances (Å) and Angles (deg) for $CaNa_2MnDPDP{\cdot}21H_2O$

| | | | |
|---|---|---|---|
| | Distances | | |
| Mn–O1 | 2.095 (2) | C2–N1 | 1.334 (3) |
| Mn–O2 | 2.160 (2) | C4–N1 | 1.349 (4) |
| Mn–O8 | 2.084 (3) | C4–C5 | 1.359 (4) |
| Mn–O9 | 2.160 (2) | C5–C6 | 1.505 (3) |
| Mn–N2 | 2.329 (2) | C6–O4 | 1.427 (3) |
| Mn–N4 | 2.348 (3) | C5–C7 | 1.408 (3) |
| P1–O4 | 1.606 (3) | C7–C8 | 1.511 (4) |
| P1–O5 | 1.503 (2) | C9–C10 | 1.520 (3) |
| P1–O6 | 1.496 (2) | C10–O2 | 1.268 (3) |
| P1–O7 | 1.503 (3) | C10–O3 | 1.235 (3) |
| P2–O11 | 1.611 (2) | C21–O8 | 1.308 (3) |
| P2–O12 | 1.508 (5) | C21–C22 | 1.401 (4) |
| P2–O13 | 1.509 (2) | C21–C27 | 1.409 (4) |
| P2–O14 | 1.508 (2) | C22–C23 | 1.479 (4) |
| N2–C8 | 1.488 (3) | C22–N3 | 1.348 (3) |
| N2–C9 | 1.488 (3) | C24–N3 | 1.345 (3) |
| N2–C11 | 1.481 (3) | C24–C25 | 1.368 (4) |
| N4–C28 | 1.490 (3) | C25–C26 | 1.514 (4) |
| N4–C29 | 1.475 (3) | C26–O11 | 1.446 (3) |
| N4–C31 | 1.484 (4) | C25–C27 | 1.391 (3) |
| C1–O1 | 1.302 (3) | C27–C28 | 1.509 (3) |
| C1–C2 | 1.416 (3) | C29–C30 | 1.494 (3) |
| C1–C7 | 1.410 (3) | C30–O9 | 1.265 (3) |
| C2–C3 | 1.472 (3) | C30–O10 | 1.245 (3) |
| | Angles | | |
| O1–Mn–O2 | 93.67 (6) | N1–C4–C5 | 119.7 (2) |
| O1–Mn–O8 | 115.27 (9) | C4–C5–C6 | 119.5 (2) |
| O1–Mn–O9 | 87.22 (6) | C4–C5–C7 | 119.2 (2) |
| O1–Mn–N2 | 86.74 (6) | C6–C5–C7 | 121.3 (2) |
| O1–Mn–N4 | 173.46 (6) | C5–C6–O4 | 110.2 (3) |
| O2–Mn–O8 | 75.08 (6) | P1–O4–C6 | 121.3 (2) |
| O2–Mn–O9 | 173.46 (6) | C5–C7–C1 | 120.1 (2) |
| O2–Mn–N2 | 75.08 (6) | C1–C7–C8 | 118.1 (2) |
| O2–Mn–N4 | 102.58 (7) | C5–C7–C8 | 121.8 (2) |
| O8–Mn–O9 | 98.35 (6) | C7–C8–N2 | 111.2 (2) |
| O8–Mn–N2 | 152.79 (8) | C8–N2–C9 | 112.9 (2) |
| O8–Mn–N4 | 85.77 (8) | C8–N2–C11 | 109.6 (2) |
| O9–Mn–N2 | 98.52 (6) | C9–N2–C11 | 110.8 (2) |
| O9–Mn–N4 | 74.44 (6) | N2–C9–C10 | 113.6 (2) |
| N2–Mn–N4 | 78.41 (8) | C9–C10–O2 | 118.7 (2) |
| O4–P1–O5 | 107.8 (2) | C9–C10–O3 | 118.8 (2) |
| O4–P1–O6 | 100.63 (10) | O2–C10–O3 | 122.5 (2) |
| O4–P1–O7 | 108.4 (2) | N2–C11–C31 | 110.0 (2) |
| O5–P1–O6 | 114.64 (11) | C11–C31–N4 | 110.1 (2) |
| O5–P1–O7 | 110.96 (10) | C31–N4–C29 | 111.7 (2) |
| O6–P1–O7 | 113.59 (10) | C31–N4–C28 | 108.9 (2) |
| O11–P2–O12 | 107.32 (14) | C29–N4–C28 | 112.7 (2) |
| O11–P2–O13 | 106.24 (9) | N4–C29–C30 | 114.0 (2) |
| O11–P2–O14 | 103.07 (9) | C29–C30–O9 | 119.2 (2) |
| O12–P2–O13 | 112.51 (10) | C29–C30–O10 | 119.2 (2) |
| O12–P2–O14 | 113.22 (12) | O9–C30–O10 | 121.6 (2) |
| O13–P2–O14 | 113.56 (10) | N4–C28–C27 | 112.6 (2) |
| Mn–O1–C1 | 124.16 (14) | C28–C27–C21 | 118.2 (2) |
| Mn–O2–C10 | 121.74 (14) | C28–C27–C25 | 122.1 (2) |
| Mn–O8–C21 | 126.4 (2) | C21–C27–C25 | 119.7 (2) |
| Mn–O9–C30 | 121.39 (14) | C27–C21–O8 | 123.2 (3) |
| Mn–N2–C8 | 107.1 (2) | C27–C21–C22 | 118.8 (2) |
| Mn–N2–C9 | 110.71 (13) | O8–C21–C22 | 118.0 (3) |
| Mn–N2–C11 | 105.44 (12) | C21–C22–C23 | 121.8 (2) |
| Mn–N4–C28 | 108.3 (2) | C21–C22–N3 | 118.6 (2) |
| Mn–N4–C29 | 110.2 (2) | C23–C22–N3 | 119.6 (2) |
| Mn–N4–C31 | 104.69 (12) | C22–N3–C24 | 123.6 (2) |
| O1–C1–C2 | 119.0 (2) | N3–C24–C25 | 119.8 (2) |
| O1–C1–C7 | 123.0 (2) | C24–C25–C26 | 117.1 (2) |
| C2–C1–C7 | 118.0 (2) | C24–C25–C27 | 119.6 (2) |
| C1–C2–C3 | 122.0 (2) | C27–C25–C26 | 123.3 (2) |
| C1–C2–N1 | 118.5 (2) | C25–C26–O11 | 110.8 (2) |
| C3–C2–N1 | 119.5 (2) | P2–O11–C26 | 117.58 (13) |
| C2–N1–C4 | 124.6 (2) | | |

computer program that displays the data in tabular form concurrent with an on-screen high-resolution plot.

Stability constants for $MnDPDP^{6-}$, $ZnDPDP^{6-}$, and $CuDPDP^{6-}$, as well as the protonated forms of the complexes, were determined by direct titration. While the $Mn^{2+}$ and $Zn^{2+}$ complexes of DPDP are nearly completely dissociated at pH 2, the data for the $Cu^{2+}$ system revealed the complex to be only ca. 6% dissociated at pH 2. In addition, the equilibrium constant for the formation of $FeDPDP^{5-}$ was expected to be greater than $10^{30}$, which would yield <1% of the complex dissociated at pH 2. Therefore, $CuDPDP^{6-}$ and $FeDPDP^{5-}$ were also studied by using a ligand–ligand competition titration. In this experiment a 1:1:1 molar

**Scheme I.** Synthesis of DPDP

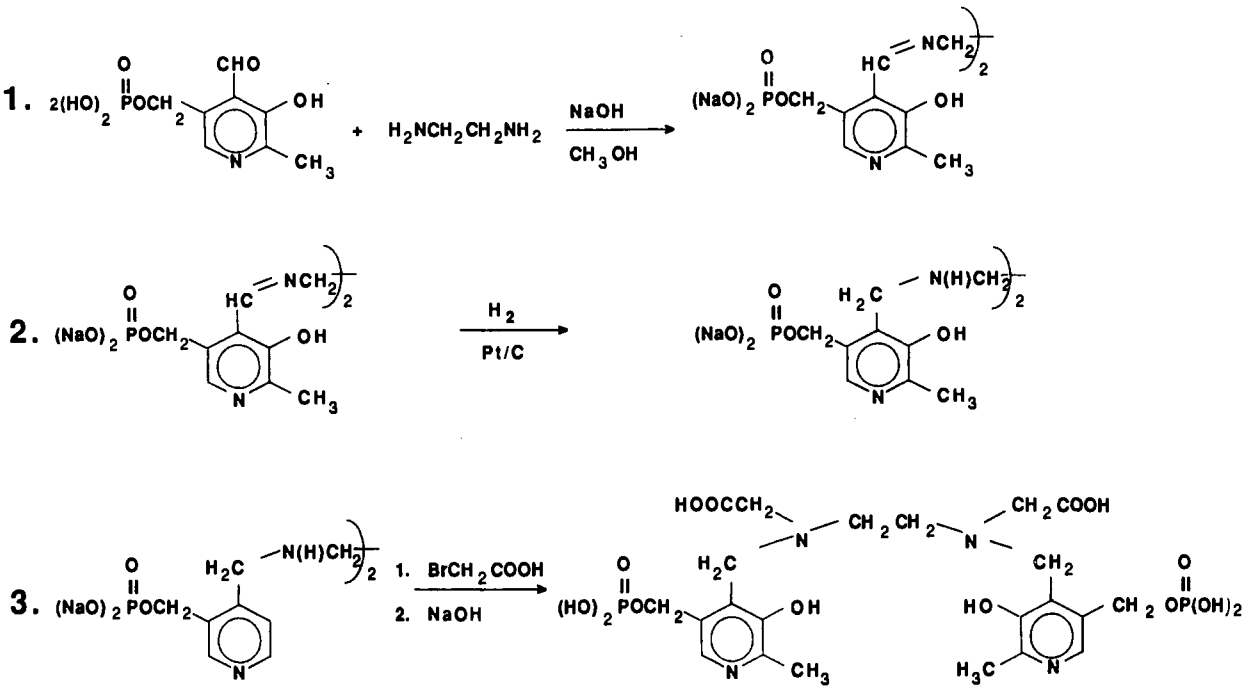


**Table IV.** Short Mn–Water Distances (Å) in $CaNa_2MnDPDP{\cdot}21H_2O$[a]

| Mn–O(water) | dist | sym code |
|---|---|---|
| Mn–O15 | 3.761 (2) | $x, y, z$ |
| Mn–O15 | 4.653 (3) | $^1/_2 - x, y - ^1/_2, ^1/_2 - z$ |
| Mn–O16 | 4.644 (5) | $x, y, z$ |
| Mn–O16 | 3.735 (6) | $^1/_2 - x, y - ^1/_2, ^1/_2 - z$ |
| Mn–O17 | 4.793 (2) | $^1/_2 - x, y - ^1/_2, ^1/_2 - z$ |
| Mn–O18 | 4.822 (2) | $x, y, z$ |

[a] Mn–O(water) distance shorter than 5.0 Å.

ratio of metal ion, DPDP, and a reference ligand was titrated. The reference ligand must form a complex with the metal ion and must have an accurately known stability constant. It is also necessary that the reference ligand be chosen such that the metal ion transfers significantly between the two ligands during the course of the titration and that hydrogen ion is either consumed or liberated during this transfer. In addition, the rate of metal ion transfer must be fast enough to ensure that equilibrium is reached in a reasonable amount of time. For $CuDPDP^{6-}$ and $FeDPDP^{5-}$, EDTA was found to be an excellent reference ligand.

**Computations.** Proton association constants for DPDP were calculated by a BASIC computer program written for polyprotic weak acid equilibrium calculations. The stability constants of the metal ion complexes were calculated by a BASIC program designed for metal ion, ligand, and proton containing a variety of species. Both programs employ a modified Newton–Raphson algorithm that calculates $-\log [H^+]$ at each point of the titration. Values for the equilibrium constants were obtained by a Simplex/Marquardt nonlinear regression algorithm that minimizes the sum of the squared differences between calculated and observed $-\log [H^+]$ values. In all titrations the average difference between observed and calculated $-\log [H^+]$ values was $<0.02$.

**NMR Measurements.** Proton nuclear magnetic resonance spectra were recorded on a Bruker AM250 spectrometer at an ambient temperature of 21 °C ± 1 °C. Solutions of DPDP and ZnDPDP were made at a concentration of 100 mM adjusted to an ionic strength of 1.0 M (NaCl).

For the NMR pH titrations, the pD of the solutions was measured with a semimicro combination electrode. The electrode was calibrated with aqueous buffer standards and then equilibrated in $D_2O$. From measured pD values the pH was calculated by the relationship

$$pH = pD - 0.40$$

which has been shown to hold for a variety of experimental conditions.[23]

**Magnetic Measurements.** The spin-only magnetic moment of MnDPDP was determined by using a modified version of the NMR method described by Evans.[24] The samples were prepared in $D_2O$ with 2% acetone at pD = 6.5. A MnDPDP concentration of 29.41 mM provided a 455-Hz difference between the acetone resonances in the inner and outer NMR tubes. The $3/(2\pi)$ shape factor in the original Evans method is only applicable to electromagnets, and a $3/(4\pi)$ shape factor is required for a superconducting magnet when concentric NMR tubes are used.

## Results and Discussion

**Synthesis of DPDP and Complexes.** The synthesis of *N,N'*-dipyridoxylethylenediamine-*N,N'*-diacetic acid 5,5'-bis(phosphate), DPDP, was undertaken in order to prepare highly water-soluble paramagnetic transition-metal chelates that might be applicable as contrast agents in MRI applications.[25] The nonphosphorylated ligand PLED was first reported by Martell and co-workers.[26] Our initial studies of the paramagnetic manganese(II) complex of PLED found this complex to have unacceptable water solubility for in vivo applications.[1]

In part for this reason, the phosphorylated ligand DPDP was synthesized (as shown in Scheme I). While this compound is not appreciably water soluble as the free acid, it readily forms 1.0 M solutions upon the addition of 4 equiv of base. This novel ligand forms highly stable coordination complexes with both 2+ and 3+ transition-metal ions; these complexes are formed via the addition of a metal halide, or other suitable metal precursor, to a neutral-pH solution of DPDP, followed by the addition of base (hydroxide, amine, etc.) to return to neutral pH. Of particular interest to us, in the context of MRI contrast enhancement, is the stable manganese(II) complex MnDPDP.

**Description and Discussion of the Structure.** The anionic complex $MnDPDP^{4-}$ and its crystallographic numbering scheme is shown in Figure 1. The asymmetric unit contains 1 complex anion, 1 calcium cation, 2 sodium cations, and 21 water molecules (Figure 2; only coordinating water molecules are shown, O15–O25). Two of the water molecules (O32, O35) are located on 2-fold axes (Wyckoff position e), bringing the number of different water *positions* to 22. The calcium and sodium cation coordination spheres include oxygen atoms from adjacent asymmetric units

(23) Covington, A. K.; Paabo, M.; Robinson, R. A.; Bates, R. G. *Anal. Chem.* **1968**, *40*, 700.
(24) Evans, D. F. *J. Chem. Soc.* **1959**, 2003–2005.
(25) Lauffer, R. B. *Chem. Rev.* **1987**, *87*, 901–927.
(26) Taliaferro, C. H.; Motekaitis, R. J.; Martell, A. E. *Inorg. Chem.* **1984**, *23*, 1188–92.
(27) Shannon, R. D. *Acta Crystallogr.* **1976**, *A32*, 751.

(O9*, O10*, O24′, O6″; Figure 3). The anion, cations, and water molecule form an indefinite polymeric network via various hydrogen bonds and coordination of oxygen atoms to the cations in the crystal lattice.

The manganese atom in the anion is in the +2 oxidation state. This is confirmed from the charge inventory, the magnetic susceptibility measurements, and the structural parameters. The fully deprotonated DPDP ligand has an 8- charge (2- on each of the $OPO_3$ groups, 1- on each of the phenolic groups, and 1- on each of the carboxylic acid groups). The two pyridine nitrogens (N1, N3) are protonated, leaving a net charge of 6-. These charges are balanced by the $Ca^{2+}$, two $Na^+$, and $Mn^{2+}$ cations. NMR measurements of magnetic susceptibility yielded a spin-only value of 5.93 $\mu_B$ (theoretical value for high-spin $Mn^{2+}$ is 5.92 $\mu_B$).

The metal coordination site is a distorted octahedron made up of two phenolate oxygen atoms, two carboxylate oxygen atoms, and two tertiary nitrogen atoms (N2, N4), as illustrated in Figure 1. The Mn–O(phenolic) and Mn–N distances of **1** are very similar to those in the earlier MnPLED structure[1] [Mn–O(phenolic) = 2.095 (2) and 2.084 (3) Å versus 2.0907 (8) Å for MnPLED; Mn–N = 2.329 (2) and 2.348 (3) Å versus 2.3513 (10) Å for MnPLED]. The only significant difference is found in the Mn–O(carboxylic acid) distances [Mn–O(carboxylic acid) = 2.160 (2) and 2.160 (2) Å versus 2.2434 (9) Å for MnPLED]. These distances are longer in the MnPLED structure, where the carboxylic acid oxygen atom is involved in a strong hydrogen bond (O6–HW4–O3), while the same atoms in **1** (O2, O9) coordinate to the calcium cation. This is consistent with the general observation that there is more single/double bond localization in carboxylic acids, for example, than in coordinated carboxylate groups.

The bond angles around manganese are also similar for the two $Mn^{2+}$ complexes. The oxygen atoms of the carboxylic acid groups are trans to each other; O3–Mn–O3′ = 176.20 (4)° versus O2–Mn–O9 = 176.40 (6)° for MnPLED and **1**, respectively. The phenolic oxygen atoms are trans to the coordinating tertiary nitrogen atom; O1–Mn–N2′ = 150.29 (3)° versus O1–Mn–N4 = 154.20 (7) and 08–Mn–N2 = 152.79 (8)° for MnPLED and **1**, respectively. All other bond distances and angles in the coordinated PLED and DPDP ligands are very similar.

The crystal structure of **1** contains two different types of counterions (Ca, Na) with three different coordination environments. The coordination geometry around calcium can be approximated as tetragonal antiprismatic (Figure 3). Atom Na1 is coordinated in a distorted octahedral fashion, while Na2 is pentacoordinate in a trigonal bipyramid (Figure 3).

There are at least 22 different hydrogen bonds (Table IVS) in the crystal lattice of **1**. A complete discussion of the hydrogen-bonding network is precluded, since not all of the water hydrogen atoms were identified in difference Fourier maps. A calculation of the least-squares planes of the aromatic rings in **1** is presented in Table VS. This calculation shows these rings are almost exactly planar, with a dihedral angle of 20.53 (4)°. The angles around the tertiary nitrogen atoms in the PLED and DPDP ligands lie in the same range, 109.76 (9)–110.79 (9)° versus 108.9 (2)–112.9 (2)°, respectively. However, the torsion angles of the N–C–C–N backbone of the ligand are significantly different for MnPLED and **1**; N2–C11–C11′–N2′ = 64.19 (14)° versus N2–C11–C31–N4 = 65.8 (4)°, respectively.

Although **1** crystallizes with 21 water molecules per Mn(II), only a few of these are near the paramagnetic manganese atom. A list of water oxygen atoms within a radius of 5 Å around the manganese atom is presented in Table IV. All water molecules within this radius also coordinate via their oxygen atoms to the calcium cation (O15–O18 and symmetry-related atoms).

As noted for the PLED structure,[1] and compared herein, the Mn–O and Mn–N bond distances are typical for Mn(II) (high spin; $r_{Mn^{2+}}$ = 0.830 Å[4] predicts a $Mn^{2+}$–O distance of 2.180 Å). The observed Mn–O distances in **1** are in good agreement with those in comparable complexes cited earlier.[28-31]

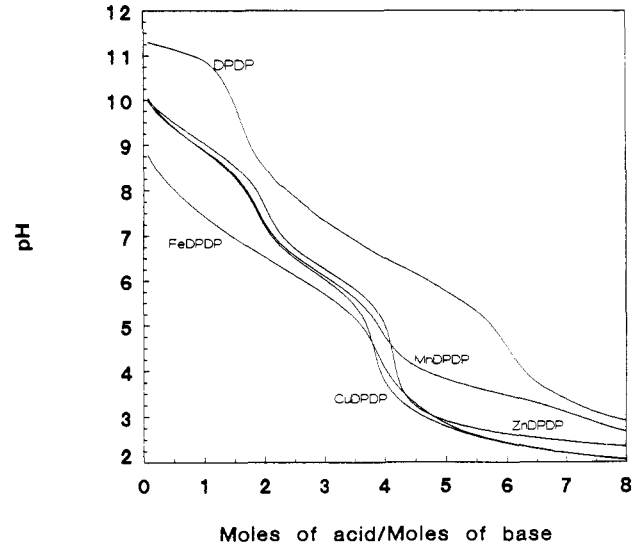


**Figure 4.** Potentiometric titration curves of DPDP in the absence and presence of equimolar $Mn^{2+}$, $Zn^{2+}$, $Cu^{2+}$, or $Fe^{3+}$. Concentration of metal ion and ligand = 4.00 × $10^{-3}$ M ($\mu$ = 0.10 M (NaCl), $T$ = 25 °C).

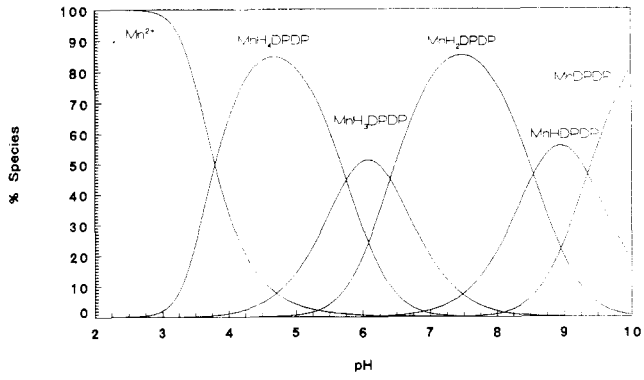


**Figure 5.** Distribution of species as a function of pH for 1 × $10^{-3}$ M MnDPDP ($\mu$ = 0.10 M (NaCl), $T$ = 25 °C).

**Potentiometric Measurements.** The potentiometric titration curves for $DPDP^{8-}$, $MnDPDP^{6-}$, $ZnDPDP^{6-}$, $CuDPDP^{6-}$, and $FeDPDP^{5-}$ are shown in Figure 4. The titration curves for $MnDPDP^{6-}$, $ZnDPDP^{6-}$, and $CuDPDP^{6-}$ show two protonation steps that occur with p$K_a$'s less than 1 unit apart (log $K_{111}$, log $K_{121}$) followed by another set of two protonations that have similar p$K_a$'s (log $K_{131}$, log $K_{141}$). These results are consistent with the first and second protonations on the divalent metal ion complexes of DPDP occurring on the pyridine nitrogens and the third and fourth protonations occurring on the phosphate groups (proton assignments are discussed in the NMR section). In contrast, $FeDPDP^{5-}$ has four protonations that are relatively evenly spaced, yielding a constant buffer capacity from pH 5 to pH 8. Thus, in $FeDPDP^{5-}$, the first and second protonations (pyridine rings) have p$K_a$'s lower than those of the divalent metal ion counterparts. The pyridine nitrogens are more acidic due to charge effects of the trivalent iron carried through the pyridine ring. The third and fourth protonations of $FeDPDP^{5-}$, however, occur with p$K_a$'s very similar to those of the divalent metal ion complexes, since these occur on the relatively isolated phosphate groups. The species distribution curve for the protonated forms of $MnDPDP^{6-}$ is shown in Figure 5. $MnH_2DPDP^{4-}$ is the predominant species at pH 7.4. At pH 3, the $MnH_4DPDP^{2-}$ complex shows considerably more dissociation than $ZnH_4DPDP^{2-}$ (Figure 4). Both $CuH_4DPDP^{2-}$

(28) Neupert-Laves, K.; Dobler, M. *Helv. Chim. Acta* **1977**, *60*, 1861–1871.
(29) Gott, G. A.; Fawcett, J.; McAuliffe, C. A.; Russell, D. R. *J. Chem. Soc., Chem. Commun.* **1984**, 1283–1284.
(30) Garrett, T. P.; Mitchell, G.; Freeman, H. C. *Acta Crystallogr.* **1983**, *C39*, 1027.
(31) A preliminary report of the Mn(pyridoxylenevalinate)$_2$ complex was never followed by the full structure analysis: Willstadter, E.; Hamor, T. A.; Hoard, J. L. *J. Am. Chem. Soc.* **1963**, *85*, 1205–1206.

**Table V.** Protonated Constants and Metal Chelate Stability Constants of DPDP and Related Ligands ($T$ = 25 °C, $\mu$ = 0.10 M (NaCl))

| equilibrium | log $K$ DPDP[a] | PLED[b] | HBED[c] |
|---|---|---|---|
| [HL]/[L][H] | 11.57 (20) | 10.75 | 12.60 |
| $[H_2L]/[HL][H]$ | 11.16 (20) | 10.33 | 11.00 |
| $[H_3L]/[H_2L][H]$ | 8.17 (9) | 7.12 | 8.44 |
| $[H_4L]/[H_3L][H]$ | 6.92 (7) | 5.64 | 4.72 |
| $[H_5L]/[H_4L][H]$ | 6.14 (8) | 3.12 | 2.53 |
| $[H_6L]/[H_5L][H]$ | 5.35 (5) | 1.74 | 1.74 |
| $[H_7L][H_6L][H]$ | 3.34 (3) | | |
| $[H_8L]/[H_7L][H]$ | 2.05 (21) | | |
| [ZnL]/[Zn][L] | 18.95 (15) | 16.68 | 18.37[d] |
| [ZnHL]/[ZnL][H] | 9.41 (3) | 8.85 | 8.27[d] |
| $[ZnH_2L]/[ZnHL][H]$ | 8.62 (2) | 8.22 | 5.99[d] |
| $[ZnH_3L]/[ZnH_2L][H]$ | 6.46 (1) | | |
| $[ZnH_4L]/[ZnH_3L][H]$ | 5.72 (1) | | |
| [CuL]/[Cu][L] | 22.08 (7) | 21.52 | 23.69 |
| [CuHL]/[CuL][H] | 9.31 (7) | 8.70 | 8.49 |
| $[CuH_2L]/[CuHL][H]$ | 8.37 (10) | 7.75 | 5.04 |
| $[CuH_3L]/[CuH_2L][H]$ | 6.43 (4) | | |
| $[CuH_4L]/[CuH_3L][H]$ | 5.64 (8) | | |
| [MnL]/[Mn][L] | 15.10 (8) | 12.56 | 14.78[d] |
| [MnHL]/[MnL][H] | 9.35 (2) | 8.74 | 7.66[d] |
| $[MnH_2L]/[MnHL][H]$ | 8.55 (4) | 7.90 | 6.58[d] |
| $[MnH_3L]/[MnH_2L][H]$ | 6.41 (1) | | |
| $[MnH_4L]/[MnH_3L][H]$ | 5.76 (1) | | |
| [FeL]/[Fe][L] | 33.52 (6) | 36.88[d] | 39.68[d] |
| [FeHL]/[FeL][H] | 7.88 (4) | 7.49[d] | |
| $[FeH_2L]/[FeHL][H]$ | 6.85 (1) | 6.59[d] | |
| $[FeH_3L]/[FeH_2L][H]$ | 6.08 (1) | | |
| $[FeH_4L]/[FeH_3L][H]$ | 5.31 (1) | | |

[a] This work. [b] Reference 1. [c] Reference 26. [d] Reference 33.

and $FeH_4DPDP^-$ show the least amount of dissociation at low pH.

The results of the potentiometric measurements for DPDP, along with those for PLED and HBED, are shown in Table V. Initially log $K$([CuL]/[Cu][L]) of 21.92 (19) for $CuDPDP^{6-}$ was determined via direct titration. However, the complex was found to be only ca. 6% dissociated at pH 2. Since accurate determination of this equilibrium constant requires that the complex be appreciably dissociated (generally near 50%)[26] at the lowest pH measured, the stability constant for $CuPLED^{6-}$ was also determined by competition titration with EDTA. The value for log $K$([CuL]/[Cu][L]) found by this potentiometric technique was 22.08 (7). The excellent agreement between the values of the stability constant obtained by both types of titrations suggests that perhaps only 10% dissociation is required for accurate determination in direct titrations if the collected data are of very high precision. In addition, we have demonstrated that the ligand–ligand competitive titration technique yields very accurate results for the DPDP/EDTA system.

Although the overall basicity of PLED is greater than that of HBED, the stability of the PLED–metal ion complexes is less than that of the HBED complexes. This is most likely due to the fact that not all the basic groups (i.e., the pyridine nitrogens) of PLED can directly participate in complexation. It has been postulated, however, that some electron density can be transferred from these groups to the participating moieties.[32] The two most basic groups of DPDP (assigned to the aliphatic amine groups as discussed later) show increased basicity over those of PLED. This increased basicity leads to enhanced stability for $Zn^{2+}$, $Cu^{2+}$, $Mn^{2+}$, and $Fe^{3+}$ DPDP complexes over those for PLED complexes, but the DPDP complexes are comparable in stability to those of HBED.[33]

At pH 7.4, the metal ion complexes of DPDP coordinate two protons on the pyridine nitrogens. Unlike those of PLED, DPDP chelates can bind two more protons on the phosphate groups before dissociation of the complex occurs. As a result of these stable protonated complexes, the conditional stability of the DPDP complexes in neutral and acidic media is enhanced.

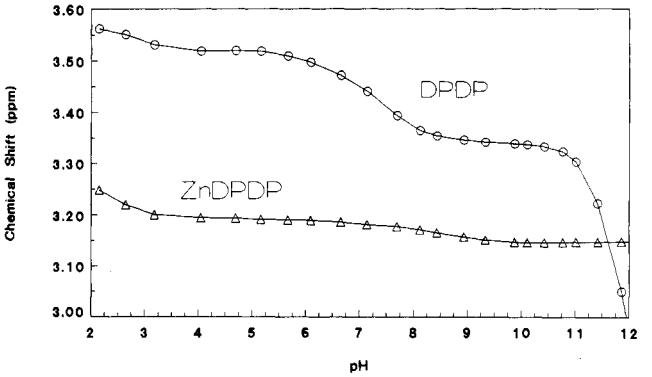


**Figure 6.** pH dependence of the chemical shift ($^1$H NMR, 250 MHz) of acetate hydrogens of (○) DPDP and (△) ZnDPDP. Solutions were 0.10 M in DPDP and ZnDPDP ($\mu$ = 1.0 M (NaCl), $T$ = 21 °C).

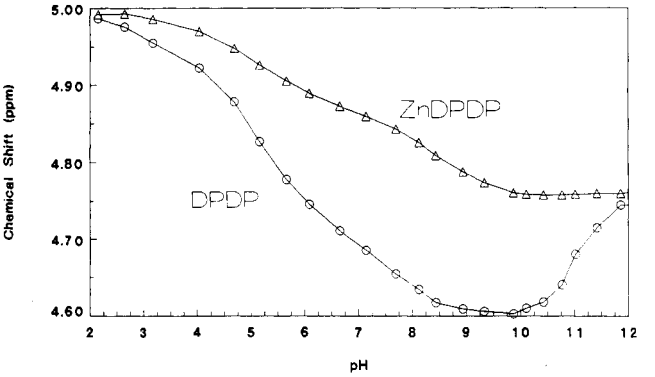


**Figure 7.** pH dependence of the chemical shift ($^1$H NMR, 250 MHz) of methylene phosphate hydrogens of (○) DPDP and (△) ZnDPDP. Solutions were 0.10 M in DPDP and ZnDPDP ($\mu$ = 1.0 M (NaCl), $T$ = 21 °C).

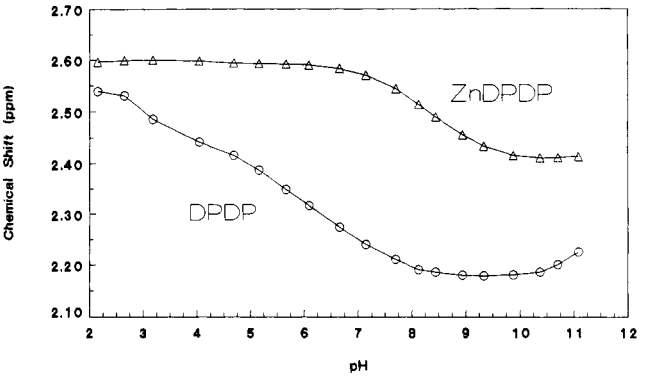


**Figure 8.** pH dependence of the chemical shift ($^1$H NMR, 250 MHz) of pyridine methyl hydrogens of (○) DPDP and (△) ZnDPDP. Solutions were 0.10 M in DPDP and ZnDPDP ($\mu$ = 1.0 M (NaCl), $T$ = 21 °C).

**NMR Studies.** Using pyridoxamine and pyridoxal 5-phosphate as representative molecules, one would expect the most basic groups in DPDP to be the aliphatic nitrogens, followed by the pyridine nitrogens. NMR studies by Martell and co-workers have indicated the pyridine nitrogens to be the most basic groups in PLED.[26] This is evident by the first two protonations in PLED causing a marked chemical shift in all substituents of the pyridine ring while not affecting the chemical shift of the acetate hydrogens. In order to differentiate aliphatic and pyridine nitrogen protonation in DPDP, a pH-dependent $^1$H NMR study was performed.

The first two protonations of DPDP greatly affect the chemical shift of the acetate hydrogens (Figure 6) and thus are assigned to aliphatic amine groups. To a lesser extent, these protonations also affect the chemical shift of the pyridine ring substituents,

(32) Choppin, G. R. *J. Less-Common Met.* **1985**, *112*, 193.
(33) L'Eplattenier, F. L.; Murase, I.; Martell, A. E. *J. Am. Chem. Soc.* **1967**, *89*, 837–843.
(34) Taliaferro, C. H.; Martell, A. E. *Inorg. Chem.* **1985**, *24*, 2408–2413.

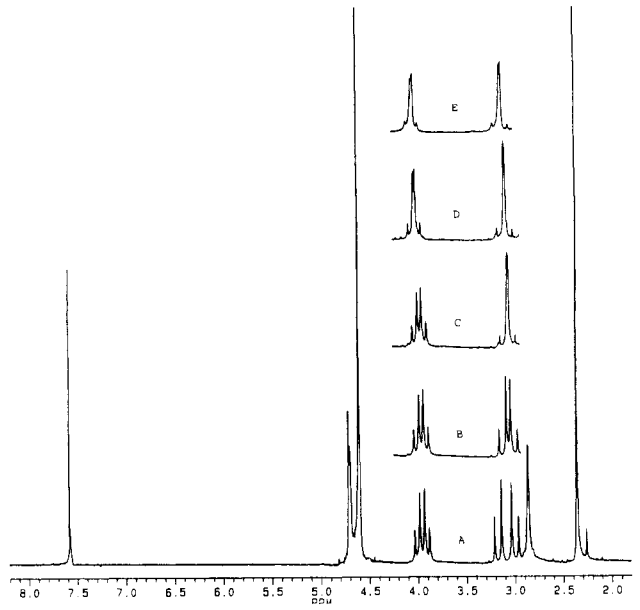


**Figure 9.** pH dependence of the ZnDPDP NMR spectrum ($^1$H, 250 MHz): (A) fully deprotonated complex at pH 10, acetate (ca. $\delta$ 3.1) and 4-$CH_2$ hydrogens (ca. $\delta$ 4.0) showing nonequivalence; (B, C) complex at pH 8.2 and 7.8, acetate hydrogens coalescing as pyridine nitrogens are protonated; (D, E) complex at pH 4.0 and 2.5, 4-$CH_2$ hydrogens coalescing as complex begins to dissociate.

presumably from hydrogen bonding of the protonated aliphatic amines to the deprotonated phenolic oxygens. The next six protonations produce large continual chemical shifts in all ring substituents, making it very difficult to differentiate protonation of the aromatic nitrogens, phosphate oxygens, and the phenolic oxygens. This is illustrated by Figure 8, which shows a progressive downfield chemical shift for the methyl group on the pyridine ring from pH 8 to pH 2. From the protonation sequence of pyridoxal 5-phosphate[35] and chemical analogy, one might assign the remaining six protonations to the two aromatic nitrogens, to each of the phosphates, and to the two phenolic oxygens. However, this sequence of protonation reactions does not seem to be obvious from the NMR data. The remaining two oxygens of the phosphate groups would not be expected to be protonated above pH 2.

The pH behavior of the chemical shifts of $ZnDPDP^{6-}$ was studied in order to elucidate the protonation sequence of the metal ion complexes of DPDP. As seen in Figures 7 and 8, the first two protonations (between pH 10 and pH 7) produce chemical shifts in both the methylene phosphate and pyridine methyl hydrogens. Thus it seems evident that the first two protonations occur on the aromatic nitrogens of the complex. The next two protonations (between pH 7 and pH 4) do not affect the pyridine methyl hydrogens (Figure 8) while producing a significant chemical shift in the methylene phosphate hydrogens (Figure 7). This is consistent with the third and fourth protonations taking place on the phosphate groups. Protonation of the phosphate groups would not be expected to affect other ring substituents because the phosphate protonation sites are not directly bonded to the pyridine ring.

The NMR spectrum of $ZnDPDP^{6-}$, shown in Figure 9, indicates that both the acetate and the 4-$CH_2$– hydrogens show nonequivalence in the deprotonated complex from the AB splitting pattern ($J_{AB}$ = 12.5 Hz for 4-$CH_2$– and $J_{AB}$ = 17.5 Hz for acetate hydrogens). This indicates that the ethylene backbone is rigid on the NMR time scale. As the pH is lowered, the acetate protons become equivalent in the NMR spectrum, collapsing to a singlet once the pyridine nitrogens are protonated. Thus, it seems that protonation of the pyridine nitrogens increases the lability of the acetate groups. Protonation of the pyridine nitrogens and phosphates on the complex does not affect the splitting pattern of the 4-$CH_2$– hydrogens. When the pH is lowered to 4.0, the 4-$CH_2$– hydrogens begin coalesence. This is also the pH where, according to the potentiometric data, the complex is known to begin dissociation. Since the 4-$CH_2$– carbon atoms are part of the chelate backbone structure, the 4-$CH_2$– hydrogen atoms do not become equivalent until the complex dissociates. The pH range of complex dissociation derived from the NMR data agrees well with the potentiometric data.

**Concluding Remarks.** Paramagnetic metal ions are known to reduce the relaxation times of nuclei in the surrounding environment because of the strong electron–nucleus magnetic moment interaction. This physical principle is the basis for the development of new and clinically useful drugs, called magnetopharmaceuticals, to be given to patients in conjunction with an NMR whole-body-imaging procedure. The image intensity in magnetic resonance imaging (MRI) is dependent upon proton density, motion, and nuclear relaxation times.[36] The administration of paramagnetic substances should enhance diagnostic MRI by (1) increasing delineation of structures in the body, (2) increasing the image contrast between normal and diseased tissue, and (3) reflecting the status of organ function or blood flow. The in vivo performance of paramagnetic contrast agents for MRI applications is evaluated by profiling the toxicology, relaxivity, biodistribution, and clearance of a promising paramagnetic chelate. The results of these biological studies lead to an understanding of the potential efficacy of a particular chelate.

MnDPDP has been found to be nontoxic in mice at 150 times the dose needed for effective liver imaging. Biodistribution studies were determined via both tissue relaxation measurements and $^{54}$Mn radiolabeling in rats. These studies indicate that MnDPDP is primarily an extracellular agent that does not cross the intact blood–brain barrier and is excreted by the kidney and liver.[37] In the absence of DPDP essentially *no* renal excretion of $^{54}$Mn ion was observed. At pharmacological doses of $^{54}$MnDPDP significant urinary levels were observed (ca. 43% within 6 h post-dose), which indicates that the chelate or a yet to be determined metabolite is excreted. The remainder of the injected dose is found in the feces (ca. 47%) and whole body (ca. 5%) at 7 days post-dose.[38]

Preliminary MRI experiments have demonstrated that MnDPDP can be used to increase the differentiation between normal and abnormal brain tissue and between metastatic cancer and normal liver parenchyma in animal models.[39] Additionally, the uptake of MnDPDP, or a metabolite, by normal cardiac tissue suggests utility in evaluating human cardiovascular status.[40,41]

The enhancement of water proton relaxivity by MnDPDP is greater than that expected for a fully coordinated manganese complex (ca. 35% greater relaxation rate than those for MnDTPA,[42] MnDOTA,[42] and MnNOTA[42]).[43] This seems to indicate

(35) Echevarria, G.; Garcia del Vado, M. A.; Garcia Blanco, F.; Menendez, M.; Laynez, J. *J. Solution Chem.* **1986**, *15*, 151–156.

(36) Valk, J.; MacLean, C.; Algra, P. R. *Basic Principles of Nuclear Magnetic Resonance Imaging*; Elsevier: Amsterdam, 1985; pp 23–26.

(37) Worah, D.; Rocklage, S. M.; Quay, S. C.; Pfefferbaum, A.; Lim, K.; Burnett, K. *Book of Abstracts*, Sixth Annual Meeting of the Society of Magnetic Resonance in Medicine; Society of Magnetic Resonance in Medicine: Berkeley, CA, 1987; Works in Progress P-16.

(38) White, D. L.; Tongol, J. M.; Roco, C. L.; Muetterties, K. A.; Engelstad, B. L.; Rocklage, S. M.; Cacheris, W. P.; Quay, S. C. *Proceedings of the 35th Annual Meeting of the Society of Nuclear Medicine*; Society of Nuclear Medicine: New York, 1988.

(39) Elizondo, G.; Tsang, Y. M.; Rocklage, S. M.; White, D. L.; Weissleder, R.; Stark, D. D.; Worah, D.; Englestad, B.; Quay, S. C.; Ferrucci, J. T. *Book of Abstracts*, Seventh Annual Meeting of the Society of Magnetic Resonance in Medicine; Society of Magnetic Resonance in Medicine: Berkeley, CA, 1988; Abstract No. 795.

(40) Saeed, M.; Wagner, S.; Wendland, M.; Derugin, N.; Pomeroy, O.; Higgins, C. B. *Book of Abstracts*, Seventh Annual Meeting of the Society of Magnetic Resonance in Medicine; Society of Magnetic Resonance in Medicine: Berkeley, CA, 1988; Abstract No. 16.

(41) Pomeroy, O. H.; Holt, W. W.; Derugin, N.; Wendland, M. F.; Quay, S.; Higgins, C. B. *Book of Abstracts*, Seventh Annual Meeting of the Society of Magnetic Resonance in Medicine; Society of Magnetic Resonance in Medicine: Berkeley, CA, 1988; Abstract No. 13.

(42) DTPA = diethylenetriaminepentaacetic acid; DOTA = 1,4,7,10-tetraazacyclododecane-*N*,*N*′,*N*″,*N*‴-tetraacetic acid; NOTA = 1,4,7-triazacyclononane-*N*,*N*′,*N*″-triacetic acid.

(43) Geraldes, C. F. G. C.; Sherry, A. D.; Brown, R. D.; Koenig, S. H. *Magn. Reson. Med.* **1986**, *3*, 242.

an enhanced interaction with the solution protons. In particular, the hydrogen-bonding network seen in the crystal structure shows that the water molecules in the outer coordination sphere of the manganese complex strongly hydrogen bond to the phosphate and pyridine nitrogen atoms. As noted in Table IV, six water molecules are less than 5 Å from the manganese center.

Studies are in progress to further assess the imaging utility of this novel chelate and to prepare a toxicity profile to support human studies. The results of these studies will be reported elsewhere.

**Acknowledgment.** We thank Steven Sheffer and Thomas Garrett for their technical assistance and helpful discussions.

**Registry No.** 1, 118248-92-3; PLP, 54-47-7; DPDP, 118248-91-2; $MnH_2DPDP^{2-}$, 118248-93-4; $MnDPDP^{6-}$, 118248-94-5; $ZnDPDP^{6-}$, 118248-95-6; $CuDPDP^{6-}$, 118248-96-7; $FeDPDP^{5-}$, 118248-97-8; $H_2NCH_2CH_2NH_2$, 107-15-3; $BrCH_2CO_2H$, 79-08-3; *N,N'*-dipyridoxylethylenediamine 5,5'-bis(phosphate), 118248-90-1.

**Supplementary Material Available:** Table IS (crystal and data collection details for $CaNa_2MnDPDP{\cdot}21H_2O$), Table IIS (hydrogen atom positional and thermal parameters), Table IIIS (bond distances and angles—a complete list), Table IVS (intramolecular and intermolecular hydrogen-bond parameters), Table VS (least-squares planes and their equations), Table VIS (anisotropic temperatures factors), and Table VIIS (root-mean-square amplitudes of thermal vibration) (11 pages); Table VIIIS (observed and calculated structure factors) (38 pages). Ordering information is given on any current masthead page.

Contribution from the Department of Chemistry,
San Jose State University, San Jose, California 95192

# Evidence for the Binding of Bromide to Mercury in Organomercurial–Protein Complexes Obtained by Using Bromine-81 Magnetic Resonance Spectroscopy

Joseph J. Pesek* and Faridah Abhanan

*Received April 19, 1988*

Bromine-81 magnetic resonance measurements are used to detect the formation of bromide–organomercurial–protein complexes. When an organomercurial compound is placed in a NaBr solution of various proteins, the bromine-81 magnetic resonance line broadens. This phenomenon can only be observed if the mercury coordination number is at least 3 with the sites being occupied by the organic moiety, the protein, and a bromide. Under these conditions quadrupolar relaxation becomes more efficient as bromide exchanges between the bound and the free states. The complexes are characterized by determining their correlation times at the binding site(s) (segmental motion) as well as the bromide ion-exchange rates. A possible fourth coordination site on mercury can be detected by adding DMSO to a NaBr solution containing the bromide–organomercury–protein complex.

Recently[1] we have reported on mercury coordination numbers greater than 2 for methylmercury and *p*-(chloromercurio)benzoic acid in the presence of 0.1 M NaCl and various proteins. This is unusual since the aqueous coordination chemistry of methylmercury and other organomercurials is usually described in terms of a linear geometry.[2] There are a few examples of methylmercury complexes with mercury coordination numbers greater than 2 such as the $CH_3HgX_2^-$ and $CH_3HgX_3^{2-}$ complexes of iodide[3] and thiocyanate.[3-5] In addition, some chelating agents such as 2,2-bipyridine have also resulted in higher coordination numbers for methylmercury.[6-10] Spectroscopic studies have shown that $CH_3HgCl_2^-$ is formed in a number of nonaqueous solvents.[11,12]

The use of halide ion NMR to study metal–protein complexes has been well established.[13] Mercury was first shown to be applicable to such investigations,[14] but zinc[15] and other metals[16] have been reported as well. For chloride, bromide, and iodide, NMR relaxation is dominated by quadrupolar effects such that the spin–lattice decay rate is given by

$$R_1 = KT_c \tag{1}$$

where $K$ is a constant that includes the spin quantum number, the electric field, and the quadrupole moment and $T_c$ is the correlation time for reorientation of the field gradient.[14] For symmetrically solvated halide ions $R_1$ values are considerably smaller (1200 $s^{-1}$ for $Br^-$) than those for covalently bound species ($>10^6$ $s^{-1}$ for Br). However if exchange occurs at a moderately fast rate between free and bound halide ions, then a single composite NMR line will be observed. The time-averaged decay rate becomes

$$R_1 = R_2 = P_f R_{1f} + P_b R_{1b} \tag{2}$$

where $R_2$ is the spin–spin relaxation rate, $P_f$ and $P_b$ are the fraction of halide ions in the free and bound forms respectively, and $R_{1f}$ and $R_{1b}$ are the relaxation rates of the free and bound halide ions respectively. For metal–protein complexes, $R_{1b} \gg R_{1f}$ (by a factor of $\sim 10^5$) so that measurable line broadening is observed at reasonable halide ion concentrations ($\sim$0.1 M) and metal–protein concentrations ($\sim 10^{-5}$ M). This large chemical amplification effect is not present when a smaller ligand is used instead of a protein. The line width increase is defined by

$$R_2 - R_{1f}/\pi = (1/k_2[B] + [X]/R_1[B])^{-1} \tag{3}$$

(1) Pesek, J. J.; Schneider, J. F. *Inorg. Chem.* **1987**, *26*, 3064.
(2) Rabenstein, D. L. *Acc. Chem. Res.* **1978**, *11*, 100.
(3) Barbieri, R.; Bjerrum, J. *Acta Chem. Scand.* **1965**, *19*, 469.
(4) Relf, J.; Cooney, R. P.; Henneike, H. F. *J. Organomet. Chem.* **1972**, *39*, 75.
(5) Petroysan, V. S.; Reutov, O. A. *J. Organomet. Chem.* **1974**, *76*, 123.
(6) Schwarzenbach, G. *Pure Appl. Chem.* **1970**, *24*, 307.
(7) Wong, Y. S.; Taylor, N. J.; Chieh, P. C.; Carty, A. J. *J. Chem. Soc., Chem. Commun.* **1974**, 625.
(8) Anderegg, G. *Helv. Chim. Acta* **1974**, *57*, 1340.
(9) Canty, A. J.; Gatehouse, B. M. *J. Chem. Soc., Dalton Trans.* **1976**, 2018.
(10) Canty, A. J.; Marker, A. *Inorg. Chem.* **1976**, *15*, 425.
(11) Lucchini, V.; Wells, P. R. *J. Organomet. Chem.* **1975**, *92*, 283.
(12) Goggin, P. L.; Goodfellow, R. J.; Hurst, N. W. *J. Chem. Soc., Dalton Trans.* **1975**, 561.
(13) Diehl, P.; Fluck, E.; Kosfeld, R. *Chlorine, Bromine, and Iodine NMR. Physico-chemical and Biological Applications*; Springer-Verlag: New York, 1976; pp 249–75.
(14) Stengle, T. R.; Baldeschweiler, J. D. *J. Am. Chem. Soc.* **1967**, *89*, 3045.
(15) Ward, R. L. *Biochemistry* **1969**, *8*, 1879.
(16) Sudmeier, J. L.; Pesek, J. J. *Anal. Biochem.* **1971**, *41*, 39.

0020-1669/89/1328-0485$01.50/0 